ARTICLE

doi:10.1038/nature12308

Temporal regulation of EGF signalling networks by the scaffold protein Shc1

Yong Zheng[1], Cunjie Zhang[1], David R. Croucher[2], Mohamed A. Soliman[1,3,4], Nicole St-Denis[1], Adrian Pasculescu[1], Lorne Taylor[1], Stephen A. Tate[5], W. Rod Hardy[6], Karen Colwill[1], Anna Yue Dai[1], Rick Bagshaw[1], James W. Dennis[1,3], Anne-Claude Gingras[1,3], Roger J. Daly[7,8] & Tony Pawson[1,3]

Cell-surface receptors frequently use scaffold proteins to recruit cytoplasmic targets, but the rationale for this is uncertain. Activated receptor tyrosine kinases, for example, engage scaffolds such as Shc1 that contain phosphotyrosine (pTyr)-binding (PTB) domains. Using quantitative mass spectrometry, here we show that mammalian Shc1 responds to epidermal growth factor (EGF) stimulation through multiple waves of distinct phosphorylation events and protein interactions. After stimulation, Shc1 rapidly binds a group of proteins that activate pro-mitogenic or survival pathways dependent on recruitment of the Grb2 adaptor to Shc1 pTyr sites. Akt-mediated feedback phosphorylation of Shc1 Ser 29 then recruits the Ptpn12 tyrosine phosphatase. This is followed by a sub-network of proteins involved in cytoskeletal reorganization, trafficking and signal termination that binds Shc1 with delayed kinetics, largely through the SgK269 pseudokinase/adaptor protein. Ptpn12 acts as a switch to convert Shc1 from pTyr/Grb2-based signalling to SgK269-mediated pathways that regulate cell invasion and morphogenesis. The Shc1 scaffold therefore directs the temporal flow of signalling information after EGF stimulation.

Many cell surface receptors associate with intracellular scaffold proteins that amplify signalling by providing docking sites for downstream effectors[1]. In the case of receptor tyrosine kinases (RTKs), autophosphorylated NXXY motifs recruit scaffolds with PTB domains, such as members of the insulin-receptor substrate (IRS), Dok, FGF-receptor substrate 2 (FRS2) and Shc families[2]. Once associated with an RTK, the scaffold is itself phosphorylated at tyrosine motifs that recruit SH2 domain proteins, resulting in the activation of intracellular pathways[3].

This begs the question as to why receptors use scaffolds for activities that might have been incorporated into the receptors themselves. We have investigated this issue using mammalian Shc1; the *Shc1* gene encodes three proteins of 46, 52 and 66 kilodaltons (kDa) that share an amino-terminal PTB domain and a carboxy-terminal SH2 domain, flanking a central region (CH1) containing two sites of phosphorylation at the adjacent Tyr 239/Tyr 240 residues, and a third site at Tyr 313 (refs 4, 5). Modification of Tyr 239 and Tyr 313 creates pYXN binding motifs for the SH2 domain of the Grb2 adaptor. Through its SH3 domains, Grb2 recruits proteins such as Sos1 and Gab1, that in turn activate the Ras-Erk MAP kinase and phosphatidylinositol-3-OH kinase PI(3)K/Akt pathways[6,7].

Shc1 is important for normal and oncogenic signalling by ErbB RTKs in mice[8–10]. *In vivo*, pTyr binding by the PTB domain is required for all known function of Shc1, but downstream signals are transmitted through both pTyr-dependent and pTyr-independent mechanisms[8,11]. Indeed, some polypeptides are known to bind Shc1 in a pTyr-independent manner, including the endocytic adaptor α-adaptin and the tyrosine phosphatase Ptpn12 (refs 12, 13). Here we demonstrate that Shc1 mediates a temporal switch in the signalling output of the EGFR.

Shc1 assembles an extensive EGF-regulated interactome

To map the dynamic properties of the EGF-regulated Shc1 signalling network, we generated Rat-2 cells stably expressing p52Shc1 doubly tagged with Flag and green fluorescent protein (GFP) (termed dt-Shc1) to a level comparable to that of the principal endogenous isoform, p52Shc1 (Supplementary Fig. 1a). Following EGF stimulation, we immunoprecipitated dt-Shc1 with anti-Flag antibodies; using mass spectrometry we identified 41 binding partners involved in cellular functions such as protein phosphorylation, lipid metabolism, endocytosis, ubiquitination and small GTPase regulation (Fig. 1). Several interactors either function in cytoskeletal rearrangement, consistent with the observation that $Shc1^{-/-}$ cells exhibit defects in focal contacts and actin stress fibres[14], or potentially antagonize Egfr mitogenic signalling. For example, the Ras GTPase activating protein (GAP) Dab2ip is a tumour suppressor that controls both Ras and NF-κB activity[15]; the atypical kinase SgK269 (also known as PEAK1) modulates the cytoskeleton to control cell spreading and migration, and thus tumorigenesis[16]; the Arf GTPase activators Asap1 and Asap2 promote cancer cell invasiveness[17,18]; and the Rho guanine nucleotide exchange factor Arhgef5 is often overexpressed in breast cancers and helps form Src-induced podosomes[19,20]. We also mapped EGF-induced phosphorylation sites on Shc1 (Ser 29, Thr 214, Tyr 239, Tyr 240, Tyr 313 and Ser 335) and Shc1-associated proteins (Fig. 1 and Supplementary Table 1).

EGF-induced dynamic phosphorylation of Shc1

To analyse the dynamics of Shc1-based signalling in EGF-stimulated cells, we developed a mass spectrometry approach based on scheduled multiple reaction monitoring (sMRM) that was quantitative and linear over four orders of magnitude[21–23] (Supplementary Figs 1–4, Supplementary Tables 2–4 and Supplementary Information). Using sMRM we mapped Shc1 phosphorylation at 16 time points covering the first 90 min following EGF stimulation. Phosphorylation of both Tyr 313 and Tyr 239/Tyr 240 peaked at 1–2 min, consistent with their being direct Egfr substrates, followed by dephosphorylation to baseline levels after 60 min (Supplementary Fig. 5a). In contrast Ser 29, Thr 214 and

[1]Samuel Lunenfeld Research Institute, Mount Sinai Hospital, 600 University Avenue, Toronto M5G 1X5, Canada. [2]Systems Biology Ireland, Conway Institute, University College Dublin, Dublin 4, Ireland. [3]Department of Molecular Genetics, University of Toronto, Toronto M5S 1A8, Canada. [4]Department of Biochemistry, Faculty of Pharmacy, Cairo University, Egypt. [5]AB SCIEX, Concord, Ontario L4K 4V8, Canada. [6]University of Massachusetts Medical School, Worcester, Massachusetts 01605, USA. [7]Department of Biochemistry and Molecular Biology, School of Biomedical Sciences, Monash University, Victoria 3800, Australia. [8]Cancer Research Program, Garvan Institute of Medical Research, Sydney, New South Wales 2010, Australia.

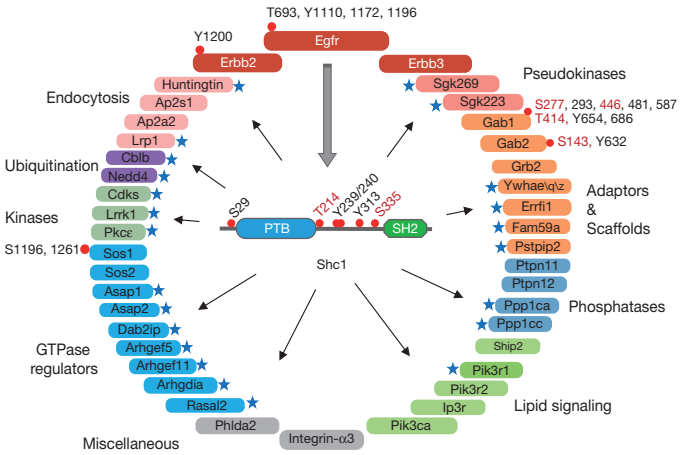

Figure 1 | EGF-dependent Shc1 phosphorylation and interactome. EGF-dependent Shc1 phosphorylation and protein interaction network identified by LC–MS in discovery mode. Novel Shc1-interacting proteins are marked by blue stars. Phosphorylation sites are shown by a red dot, with new sites highlighted in red. Proteins are coloured according to functional groups.

Ser 335 were phosphorylated with distinct kinetics (Fig. 2a and Supplementary Fig. 5b). Phosphorylation of Ser 29 started at ~40 s and peaked at 3 min, indicating that it is a substrate for a Ser/Thr kinase that is rapidly activated by the Egfr. Thr 214 phosphorylation began 1 min after EGF addition and peaked at 5 min, implicating a kinase further downstream of the receptor. Phosphorylation of Ser 335 reached a maximum only at 20 min. The totality of measured phosphorylation sites in the EGF-induced Shc1 signalling network showed a similar pattern; Tyr sites were rapidly phosphorylated followed by distinct waves of Ser/Thr phosphorylation (Fig. 2b), as revealed by principal component analysis (PCA) (Supplementary Fig. 6).

Shc1 feedback phosphorylation by Erk MAPK and Akt

Egfr phosphorylation of Shc1 stimulates the Ras-Erk MAPK and PI(3)K/Akt pathways, which may mediate Shc1 feedback phosphorylation at Ser/Thr sites. The Egfr inhibitor AG1478 abolished phosphorylation of all Shc1 Tyr and Ser/Thr sites (Fig. 2c). Shc1 Ser 29 lies in an RXXS/T substrate motif for AGC kinases, and its phosphorylation was diminished by the pan-PI(3)K inhibitor LY294002 and by a p110α PI(3)K-specific inhibitor (Fig. 2c and Supplementary Figs 7 and 8a)[24]. Treatment with an Akt kinase inhibitor (Akt inhibitor IV) specifically blocked Ser 29 phosphorylation, and Ser 29 was selectively phosphorylated by Akt *in vitro* (Supplementary Fig. 8b and Fig. 2d). In contrast, Thr 214 is followed by a proline; its phosphorylation was blocked by the MEK inhibitor PD98059 and it was selectively phosphorylated by Erk MAPK *in vitro* (Fig. 2c, d). Thus EGF stimulation initially induces Shc1 tyrosine phosphorylation, followed very rapidly by Akt-mediated Ser 29 phosphorylation, and with a slightly longer lag, phosphorylation of Thr 214 by Erk. The slower kinetics observed for Thr 214 as compared to Ser 29 phosphorylation is consistent with Erk being more distal to the Egfr than Akt, which is supported by direct analysis of Erk and Akt phosphorylation kinetics (Fig. 2e and Supplementary Fig. 9). The kinase responsible for Ser 335 phosphorylation remains to be identified (Fig. 2c, d). Kinase feedback loops therefore phosphorylate Shc1 on distinct residues, and with different kinetics, potentially affecting the nature of signalling following EGF stimulation.

The nature of Shc1 interactome switches over time

sMRM-based quantification revealed that various binding proteins associated with Shc1 with diverse kinetics. We assigned each Shc1-binding protein, except for Shcbp1, to one of three clusters, based on the time

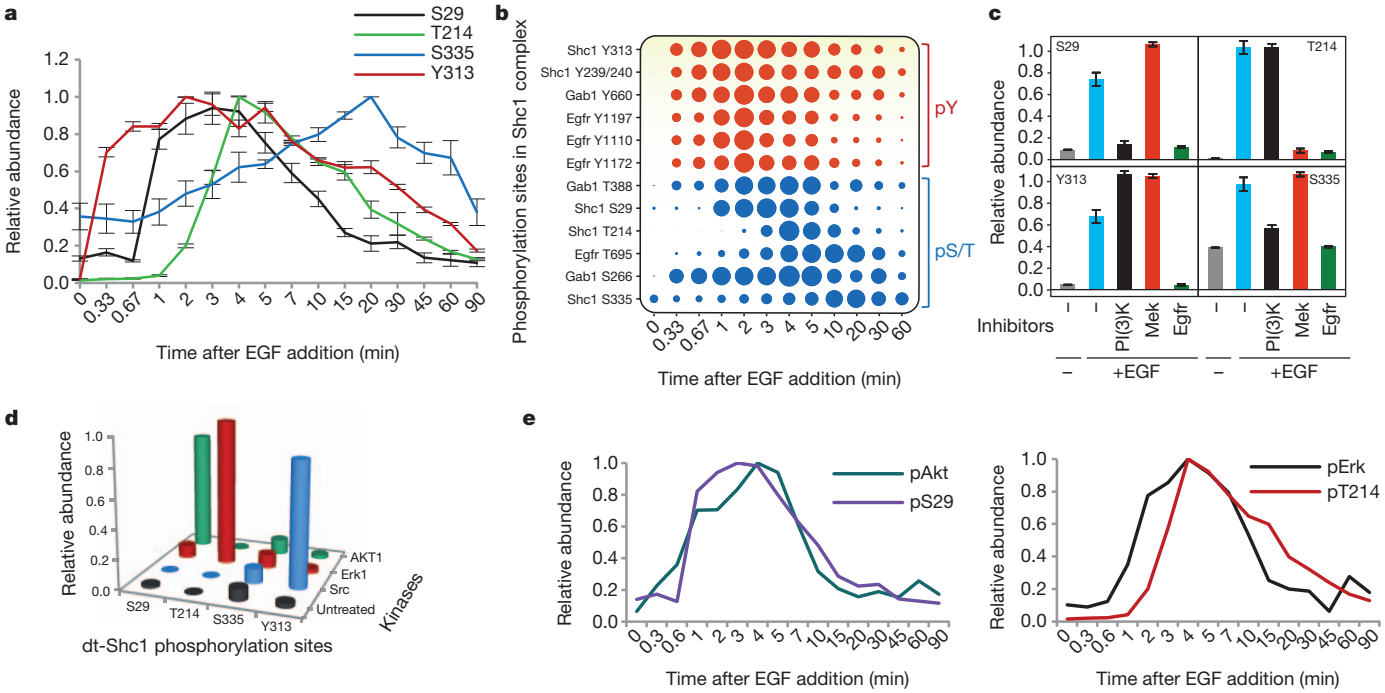

Figure 2 | Dynamic phosphorylation of Shc1 and interacting proteins. **a**, Temporal profiles of individual Shc1 phosphorylation sites following EGF stimulation. dt-Shc1 was affinity purified from EGF-stimulated fibroblasts at various time points. Relative abundance of dt-Shc1 phosphopeptides was quantified by sMRM and plotted using a quasi logarithm time scale to expand the early phase of phosphorylation. **b**, Temporal profiles of all analysed phosphorylation sites in the EGF-induced Shc1 complex. The size of each dot is proportional to the relative abundance of the corresponding phosphopeptide. **c**, Differential inhibition of Shc1 phosphorylation by kinase inhibitors as quantified by sMRM. **d**, *In vitro* kinase/sMRM analysis. Affinity purified dt-Shc1 was incubated with recombinant kinases *in vitro*. Phosphorylation of dt-Shc1 sites was quantified by sMRM. **e**, Activation kinetics of Akt and Erk1 were measured by quantitative immunoblotting, and overlaid with the phosphorylation kinetics of Shc1 S29 and T214 from **a**, respectively. Inhibitors used were Egfr: AG1478; PI(3)K: LY294002; and Mek: PD98059. Results are representative of three independent experiments. Error bars are s.d. from all transitions for a given protein/peptide from all technical repeats.

required for maximal binding (Fig. 3a and Supplementary Figs 10–14). Following EGF stimulation, Cluster 1 proteins were maximally bound to Shc1 at ~1–2 min, largely through pTyr/Grb2-dependent interactions (discussed below). This group includes ErbB receptors that bind the Shc1 PTB domain, and effectors primarily involved in stimulating the Ras-Erk MAP kinase and PI(3)K pathways, including scaffold proteins (Gab1/2, Fam59a/GAREM), Ras/Rho GEFs (Sos1/Sos2, Arhgef5), protein/lipid kinases and phosphatases (Pik3, Ptpn11, Lrrk1) and an E3 ubiquitin-protein ligase (Cblb)[25,26]. Several of these targets are new Shc1-binders, such as Arhgef5, Lrrk1 and Fam59a, potentially with positive roles in proliferation and migration[27]. Members of this group showed distinct dissociation kinetics. For example, Sos1 and Sos2 were more transiently associated with Shc1 than Grb2, potentially due to the disassembly of the Grb2/Sos complex caused by feedback phosphorylation of Sos (ref. 28). We subdivided this cluster into two groups, 1a and 1b; Cluster 1b proteins bound a few seconds more rapidly to Shc1 following EGF stimulation compared with Cluster 1a, and remained associated for longer, suggesting a more prolonged involvement in Shc1 signalling.

The tyrosine phosphatase Ptpn12, the endocytic adaptor protein Ap2 and the lipid phosphatase Ship2 comprise Cluster 2, and bound maximally to Shc1 for between 2–5 min, followed by a rather rapid disassociation. Cluster 3 proteins associate more slowly with Shc1, with binding peaking between 15–20 min. Several proteins in this cluster have been implicated in cytoskeletal reorganization, including SgK269/PEAK1, SgK223/pragmin and Asap2 (ref. 29); others, including the tumour suppressors RasGAP Dab2ip and the Ppp1ca/Ppp1cc Ser/Thr protein phosphatases, suppress Ras/MAPK signalling[15,30], and can therefore downregulate signalling induced by Cluster 1 proteins. Cluster 3 proteins share similar association/disassociation kinetics, and could

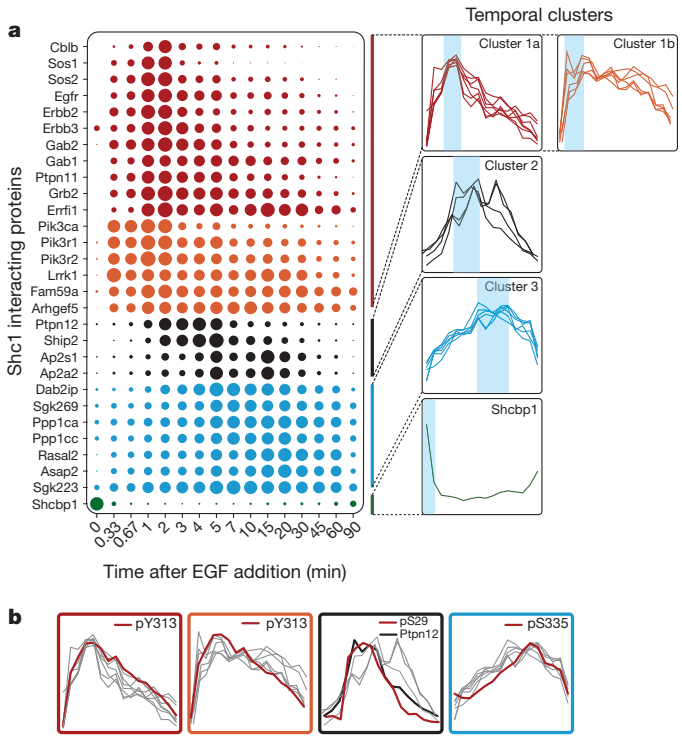

Figure 3 | Temporal profiles of the Shc1 signalling network. **a**, dt-Shc1-associated proteins were quantified as a function of time following EGF stimulation. The size of each dot is proportional to the relative abundance of the associated protein. Proteins were divided into three clusters based on the similarity of their association rates with dt-Shc1 and were colour-coded accordingly. Shcbp1 has a unique binding profile. At right, individual binding curves from each cluster were overlaid, with blue shading over the regions with maximal protein binding. **b**, Overlays of each temporal cluster with kinetic profiles of Shc1 phosphorylation sites (pY313 vs. Cluster 1a and 1b; pS29 vs. Cluster 2; pS335 vs. Cluster 3).

therefore coordinately control cell morphology, movement and proliferation. Finally, Shcbp1 is associated with Shc1 before stimulation but is displaced following EGF treatment, suggesting an inhibitory activity; indeed Shcbp1 and pTyr bind competitively to the Shc1 SH2 domain[31].

We saw a similar pattern of EGF-induced Shc1 phosphorylation and interacting proteins using primary embryonic fibroblasts from mice in which Flag-tagged *Shc1* had been knocked into the endogenous *Shc1* locus[8], indicating that the results obtained with dt-Shc1 are physiologically relevant (Supplementary Figs 15 and 16). This coordinated assembly and disassembly of Shc1 complexes suggests that Shc1 signalling properties switch during the course of growth factor stimulation from activation of the Erk/PI(3)K pathways to the control of cytoskeletal architecture, cell movement and signal reversal.

Grb2-independent late phase Shc1 complex assembly

Work on Shc1 signalling has focused on the pYXN-mediated recruitment of Grb2 (ref. 32). However, the delayed binding of Cluster 2 and 3 proteins (Supplementary Fig. 17) argues that Shc1 has Grb2-independent functions. To test this notion, we stably expressed dt-Shc1 in mouse embryonic fibroblasts (MEFs) in which the *Grb2* gene can be inducibly deleted (Supplementary Fig. 18). Binding of Cluster 1 proteins to Shc1, except for upstream RTKs, was almost completely abolished following *Grb2* deletion (Fig. 4a and Supplementary Fig. 19), indicating that Grb2 couples Shc1 pTyr sites to these targets during early EGF signalling. PCA confirmed that Shc1 tyrosine phosphorylation correlates with the binding of Cluster 1 proteins (Fig. 4b). In contrast, association of Cluster 2 and 3 proteins with Shc1 upon EGF stimulation was retained in *Grb2*-deficient cells (Fig. 4a). The delayed wave of Shc1-binders is therefore Grb2-independent, but correlates with Ser 29 and Ser 335 phosphorylation (Fig. 4b).

In the absence of Grb2 there was increased and sustained phosphorylation of Tyr 313 and Tyr 239/Tyr 240, especially during the later phase of Egfr signalling (>10-fold increase at 60 min) (Supplementary Fig. 20a). At the same time, Ser 29 and Thr 214 phosphorylation decreased by 47% and 56% (at 3 min), respectively. This argues that feedback phosphorylation of Shc1 Ser 29 and Thr 214 relies on pathways activated by Grb2-mediated signalling. Loss of Grb2 also caused an increased and prolonged tyrosine phosphorylation on the Egfr (Supplementary Fig. 20b), presumably due to failed recruitment of a tyrosine phosphatase.

To investigate whether Shc1 Ser/Thr phosphorylation sites are involved in Grb2-independent protein interactions, we quantified the Shc1 protein-interaction network in *Shc1*-null MEFs stably expressing either wild-type dt-Shc1, or dt-Shc1 mutants lacking all three phospho-Ser/Thr sites (3A) or all three pTyr sites (3F). The Shc1(3F) mutant selectively lost association with Cluster 1 proteins, consistent with lack of Grb2 recruitment. Conversely, binding to Cluster 2 and 3 proteins, except for Asap2, was reduced or abolished in the Shc1(3A) mutant (Fig. 4c and Supplementary Fig. 21). Analysis of Shc1 mutants lacking individual Ser/Thr sites indicated that this effect was largely due to loss of the Ser 29 site (Supplementary Figs 22–24). Replacing Ser 29 with alanine suppressed binding of Shc1 to the tyrosine phosphatase Ptpn12, consistent with the temporal correlation between Ser 29 phosphorylation and Ptpn12 binding (Figs 3b and 4b). Previous work has indicated that an atypical NPLH motif on Ptpn12 is recognized by the Shc1 PTB domain[33], but that stable association also requires phosphorylation of Ser 29 N-terminal to the PTB domain[13]. The depletion of Ptpn12 from the Shc1 complex observed with the Shc1 3A and S29A mutants correlated with enhanced binding of the pro-mitogenic Cluster 1 proteins (Fig. 4c and Supplementary Figs 21 and 22), probably due to increased Shc1 tyrosine phosphorylation and Grb2-binding in the absence of the Ptpn12 phosphatase, but attenuated binding of inhibitory Cluster 2 and 3 proteins. The pSer 29-dependent recruitment of Ptpn12 (a Cluster 2 protein) may therefore switch Shc1 from pro-mitogenic/survival signalling mediated by Grb2-associated Cluster 1 proteins to a form that attenuates signalling and stimulates cytoskeletal reorganization through

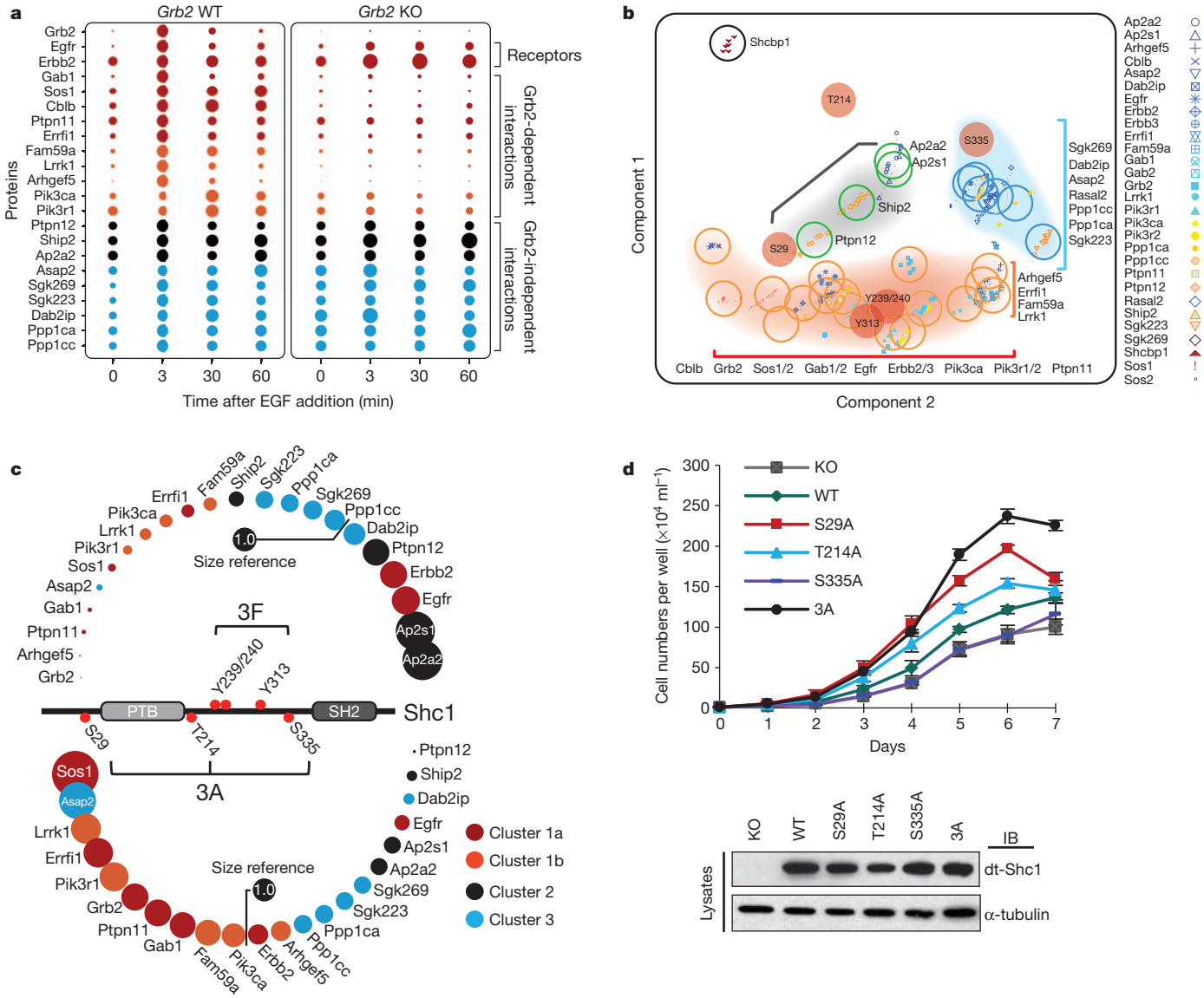

Figure 4 | Grb2-independent, serine/threonine-dependent Shc1 protein interactions. **a**, EGF-induced dt-Shc1 protein interactions were quantified by sMRM in *Grb2*$^{flox/flox}$ MEFs, with (WT, wild type) or without (KO, knockout) functional *Grb2*. Dots are coloured according to the temporal clusters defined in Fig. 3a. **b**, Correlations between Shc1 phosphorylation and protein binding revealed by PCA. The centre of each open circle marks the mean PCA value for each protein. The open circles are coloured according to the protein's cluster assignment. The red-filled circles are Shc1 phosphorylation sites. Shaded areas indicate co-modulations between specific Shc1 phosphorylation sites and binding clusters. **c**, Shc1 complex assembly in *Shc1*-deficient MEFs stably expressing wild-type dt-Shc1 compared to phosphosite mutants (3F: Y239/Y240F/Y313F; 3A: S29A/S335A/T214A) at 5 min post-EGF stimulation. The relative abundance of each protein from the wild-type dt-Shc1 complex was set at 1.0 (size reference). Changes in protein binding to Shc1 mutants are represented as the fold change over wild type. **d**, Proliferation of Shc1-deficient MEFs expressing wild type or mutant dt-Shc1 as quantified by cell counting. Bottom panel shows expression levels of dt-Shc1 variants. Error bars are ± s.d. from three technical replicates. IB, immunoblot. All results represent a minimum of three independent experiments.

Cluster 3 proteins. This is consistent with Ptpn12 acting as a tumour suppressor in human breast cancer[34].

PCA also showed that Shc1 Ser 335 phosphorylation is co-modulated with the binding of Cluster 3 proteins. However, substitution of Shc1 Ser 335 substantially decreased binding of the majority of Shc1 partners (Supplementary Fig. 23), indicating that this site may stabilize Shc1 signalling complexes. The timing of Thr 214 phosphorylation did not correlate with any of the Shc1 protein–protein interactions (Fig. 4b), and substitution of Thr 214 only marginally affected the Shc1 interactome (Supplementary Fig. 24).

The initial wave of pTyr-dependent binding proteins is therefore followed by a second network of binding partners enriched for regulators of cytoskeletal organization and cell migration, trafficking and inhibitors of mitogenic signalling. Consistent with the biochemical data, *Shc1*-null MEFs expressing the dt-Shc1(3A) mutant lacking all three Ser/Thr phosphorylation sites proliferated more rapidly than cells expressing wild-type dt-Shc1 (Fig. 4d), and cells expressing the Shc1 S29A single-site mutant showed a large increase in mitotic activity compared with the T214A or S335A mutants.

These data argue that feedback phosphorylation of Shc1 Ser 29 is particularly important for the binding of Cluster 2 and 3 proteins, including targets that negatively regulate cell growth. Erk-mediated phosphorylation of Thr 214 also restricts cell proliferation, but through a device other than recruitment of proteins analysed here.

Late phase SHC1 complex assembly by SGK269

In EGF-stimulated cells, Cluster 3 proteins bind Shc1 with similar kinetics, suggesting that their recruitment to Shc1 might be coordinated

by an adaptor other than Grb2. When we used the human PPP1CA, PPP1CB or PPP1CC isoforms as baits for affinity purification and liquid chromatography–mass spectrometry (LC–MS) analysis, we identified SGK269 as a prominent binding partner for PPP1CA and PPP1CC, but not PPP1CB (Supplementary Fig. 25a). This recalls the selective binding of Shc1 to SgK269 and Ppp1ca/Ppp1cc, which are among the Cluster 3 proteins. PPP1CA/PPP1CC did not associate with the closely related SGK223 (Supplementary Fig. 25b). These observations suggest that PPP1CA and PPP1CC might be recruited to SHC1 through SGK269, a large protein with a C-terminal pseudokinase domain and an N-terminal region with numerous potential sites of phosphorylation and predicted interaction motifs (Supplementary Fig. 26). Lentiviral-mediated short hairpin RNA (shRNA) knockdown of *SGK269* expression in HeLa cells reduced PPP1CA/PPP1CC binding to SHC1 (Supplementary Fig. 27), indicating that SGK269 acts as a bridge between PPP1CA/PPP1CC and SHC1. Surprisingly, knockingdown *SGK269* also suppressed the association of other Cluster 3 proteins with SHC1, including DAB2IP, ASAP2 and SGK223 (Fig. 5a; RASAL2 was not detectable in HeLa cells). This effect was specific to *SGK269*, as shRNA-induced silencing of *DAB2IP* expression only negatively affected the binding of ASAP2 (Supplementary Fig. 28). These data argue that SGK269 is a scaffold that enables SHC1 to switch from GRB2-dependent mitogenic activity to GRB2-independent functions. We confirmed that EGF induced binding of SGK269 to endogenous SHC1, and that this interaction increased during the late phase of EGFR signalling (Supplementary Fig. 29a).

As judged by mutagenesis experiments, phosphorylation of SGK269 Y1188, which lies in a PTB-binding NPXY motif, is necessary for binding to Shc1 (Supplementary Fig. 29b, c), indicating that tyrosine phosphorylation prompts SGK269 recognition by the SHC1 PTB domain. Using a Matrigel assay, we showed that overexpressing wild-type SGK269 in MCF-10A human epithelial breast cells generated acini that had a twofold increased diameter, a multi-lobular morphology and non-cleared lumens, while control cells formed rounded, hollow acini. In contrast, a SGK269(Y1188F) mutant that fails to bind SHC1 was relatively inactive in this assay (Fig. 5b–d and Supplementary Fig. 30). These observations support a role for the late-forming SHC1–SGK269 complex in regulating acinar morphogenesis.

Conclusion

RTKs frequently use PTB-containing scaffolds to recruit their targets. Here we define a dynamic signalling network surrounding the Shc1 scaffold for ErbB RTKs (Fig. 6). Following EGF stimulation, tyrosine phosphorylated Shc1 rapidly binds Grb2 and Grb2-associated proteins that stimulate mitogenic and survival pathways. There is subsequently a switch in the Shc1 interactome to non-SH2 domain proteins involved in cytoskeletal reorganization, trafficking and downregulation of pro-mitogenic pathways. These latter complexes are linked to Shc1 serine/threonine phosphorylation, which may be a mechanism by which Shc1 monitors the state of pathway activation following growth factor stimulation, and directs a switch in its own output accordingly.

The dynamic properties of Shc1 can be appreciated by following the successive partners for its pTyr recognition domains. Shc1 is initially associated with Shcbp1, which may inhibit the precocious association of Shc1 with other targets[31]. Following EGF stimulation, Shcbp1 is displaced as Shc1 is recruited to pTyr motifs on autophosphorylated ErbB RTKs, notably through binding of the PTB domain to NXXpY motifs; this facilitates the phosphorylation of Shc1 YXN sites, resulting in their binding to the Grb2 SH2 domain and the recruitment of Cluster 1 proteins that stimulate the Ras-Erk MAP kinase and PI(3)K-Akt pathways, favouring cell proliferation and survival. The subsequent feedback phosphorylation of Shc1 on Ser 29 by Akt recruits the tyrosine phosphatase Ptpn12 (a Cluster 2 protein), which also occupies the Shc1 PTB domain through an NPLH motif[33]. Ptpn12 antagonizes pro-mitogenic EGFR signalling, potentially by both displacing Shc1 from the EGFR and by dephosphorylating its Grb2-binding YXN motifs. Grb2 is then replaced by the SgK269 pseudokinase/scaffold that promotes the invasiveness of breast epithelial cells[35]; SgK269 binds the Shc1 PTB domain through a phosphorylated NPXY site, and brings in Ppp1c serine/threonine phosphatases and other Cluster 3 proteins. Taken together, we propose that Shc1 is a hub that determines the timing with which EGF-induced signalling switches between distinct states. This may be a more general property of scaffolds required for signalling from distinct types of cell surface receptors.

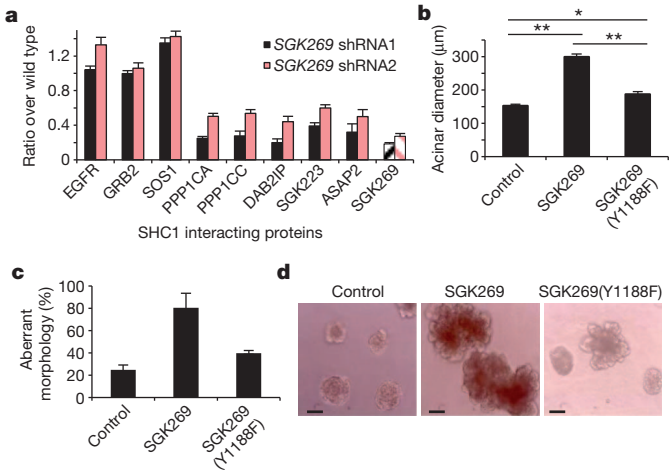

Figure 5 | SGK269 mediates late phase Shc1 protein interactions and regulates acinar morphology of breast epithelial cells in 3D culture. **a**, Cells stably infected with shRNAs for SGK269 or luciferase were stimulated with EGF. Association of SHC1 with Cluster 3 proteins and representative Cluster 1 proteins was quantified by sMRM. Error bars are ± s.d. from all transitions for a given protein/peptide from all technical repeats. Striped bars indicate the target for shRNA. **b**, **c**, Effects of the SGK269(Y1188F) mutation on acini size and morphology were analysed 12 days after inoculation into Matrigel. The diameters of ~100 acini were measured (± s.e.m., $^{**}P < 0.0001$, $^{*}P < 0.001$). Data in **a**–**c** are representative of two independent experiments. **d**, Representative images of acini. Scale bars, 100 µm.

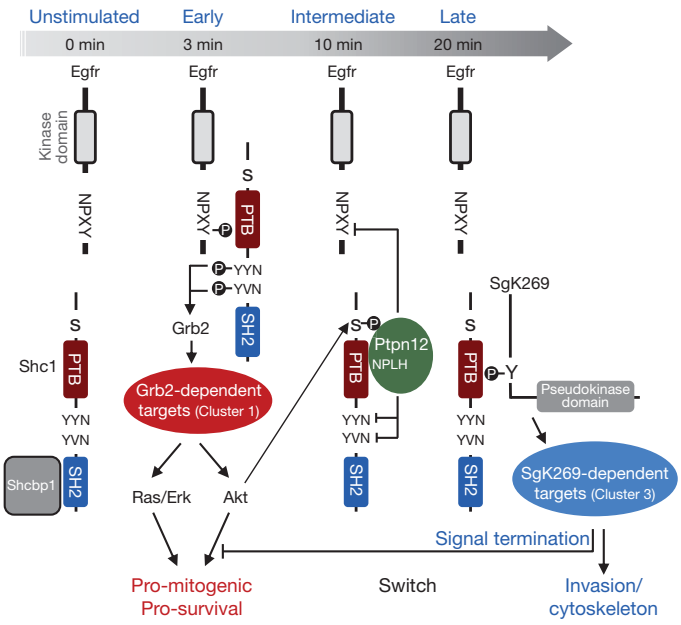

Figure 6 | Model for temporal regulation of Shc1 signalling following Egfr activation. The figure depicts the different phosphorylation events and protein interactions involving Shc1 as a function of time following EGF stimulation. See text for details.

METHODS SUMMARY

The Shc1 complexes were immunoprecipitated and digested on beads by trypsin. Shc1 interacting proteins were mapped on a TripleTOF (AB SCIEX) then quantified by sMRM on a QTRAP (AB SCIEX). MRM transitions are listed in Supplementary Table 2. Statistical analyses and presentation of MRM data were done by an in-house software pipeline programmed using R language. Genes were silenced with a lentiviral-mediated stable knockdown approach. sMRM quantification data sets from this study can be found at (http://pawsonlab.mshri.on.ca/Shc1_dynamics).

Full Methods and any associated references are available in the online version of the paper.

Received 6 July 2012; accepted 16 May 2013.

1. Good, M. C., Zalatan, J. G. & Lim, W. A. Scaffold proteins: hubs for controlling the flow of cellular information. *Science* **332,** 680–686 (2011).
2. Lemmon, M. A. & Schlessinger, J. Cell signaling by receptor tyrosine kinases. *Cell* **141,** 1117–1134 (2010).
3. Uhlik, M. T. *et al.* Structural and evolutionary division of phosphotyrosine binding (PTB) domains. *J. Mol. Biol.* **345,** 1–20 (2005).
4. Luzi, L., Confalonieri, S., Di Fiore, P. P. & Pelicci, P. G. Evolution of Shc functions from nematode to human. *Curr. Opin. Genet. Dev.* **10,** 668–674 (2000).
5. van der Geer, P., Wiley, S., Gish, G. D. & Pawson, T. The Shc adaptor protein is highly phosphorylated at conserved, twin tyrosine residues (Y239/240) that mediate protein-protein interactions. *Curr. Biol.* **6,** 1435–1444 (1996).
6. Pawson, T. Dynamic control of signaling by modular adaptor proteins. *Curr. Opin. Cell Biol.* **19,** 112–116 (2007).
7. Bisson, N. *et al.* Selected reaction monitoring mass spectrometry reveals the dynamics of signaling through the GRB2 adaptor. *Nature Biotechnol.* **29,** 653–658 (2011).
8. Hardy, W. R. *et al.* Combinatorial ShcA docking interactions support diversity in tissue morphogenesis. *Science* **317,** 251–256 (2007).
9. Dankort, D. *et al.* Grb2 and Shc adapter proteins play distinct roles in Neu (ErbB-2)-induced mammary tumorigenesis: implications for human breast cancer. *Mol. Cell. Biol.* **21,** 1540–1551 (2001).
10. Ursini-Siegel, J. *et al.* ShcA signalling is essential for tumour progression in mouse models of human breast cancer. *EMBO J.* **27,** 910–920 (2008).
11. Vanderlaan, R. D. *et al.* The ShcA phosphotyrosine docking protein uses distinct mechanisms to regulate myocyte and global heart function. *Circ. Res.* **108,** 184–193 (2011).
12. Okabayashi, Y. *et al.* Interaction of Shc with adaptor protein adaptins. *J. Biol. Chem.* **271,** 5265–5269 (1996).
13. Faisal, A., el-Shemerly, M., Hess, D. & Nagamine, Y. Serine/threonine phosphorylation of ShcA. Regulation of protein-tyrosine phosphatase-pest binding and involvement in insulin signaling. *J. Biol. Chem.* **277,** 30144–30152 (2002).
14. Lai, K. M. & Pawson, T. The ShcA phosphotyrosine docking protein sensitizes cardiovascular signaling in the mouse embryo. *Genes Dev.* **14,** 1132–1145 (2000).
15. Min, J. *et al.* An oncogene-tumor suppressor cascade drives metastatic prostate cancer by coordinately activating Ras and nuclear factor-κB. *Nature Med.* **16,** 286–294 (2010).
16. Wang, Y. *et al.* Pseudopodium-enriched atypical kinase 1 regulates the cytoskeleton and cancer progression. *Proc. Natl Acad. Sci. USA* **107,** 10920–10925 (2010).
17. Müller, T. *et al.* ASAP1 promotes tumor cell motility and invasiveness, stimulates metastasis formation *in vivo*, and correlates with poor survival in colorectal cancer patients. *Oncogene* **29,** 2393–2403 (2010).
18. Kondo, A. *et al.* A new paxillin-binding protein, PAG3/Papα/KIAA0400, bearing an ADP-ribosylation factor GTPase-activating protein activity, is involved in paxillin recruitment to focal adhesions and cell migration. *Mol. Biol. Cell* **11,** 1315–1327 (2000).
19. Kuroiwa, M., Oneyama, C., Nada, S. & Okada, M. The guanine nucleotide exchange factor Arhgef5 plays crucial roles in Src-induced podosome formation. *J. Cell Sci.* **124,** 1726–1738 (2011).
20. Debily, M. A. *et al.* Expression and molecular characterization of alternative transcripts of the *ARHGEF5/TIM* oncogene specific for human breast cancer. *Hum. Mol. Genet.* **13,** 323–334 (2004).
21. Anderson, L. & Hunter, C. L. Quantitative mass spectrometric multiple reaction monitoring assays for major plasma proteins. *Mol. Cell. Proteomics* **5,** 573–588 (2006).
22. Lange, V. *et al.* Targeted quantitative analysis of *Streptococcus pyogenes* virulence factors by multiple reaction monitoring. *Mol. Cell. Proteomics* **7,** 1489–1500 (2008).
23. Picotti, P., Bodenmiller, B., Mueller, L. N., Domon, B. & Aebersold, R. Full dynamic range proteome analysis of *S. cerevisiae* by targeted proteomics. *Cell* **138,** 795–806 (2009).
24. Knight, Z. A. *et al.* A pharmacological map of the PI3-K family defines a role for p110α in insulin signaling. *Cell* **125,** 733–747 (2006).
25. Cantley, L. C. The phosphoinositide 3-kinase pathway. *Science* **296,** 1655–1657 (2002).
26. Schlessinger, J. Common and distinct elements in cellular signaling via EGF and FGF receptors. *Science* **306,** 1506–1507 (2004).
27. Tashiro, K. *et al.* GAREM, a novel adaptor protein for growth factor receptor-bound protein 2, contributes to cellular transformation through the activation of extracellular signal-regulated kinase signaling. *J. Biol. Chem.* **284,** 20206–20214 (2009).
28. Chen, D., Waters, S. B., Holt, K. H. & Pessin, J. E. SOS phosphorylation and disassociation of the Grb2-SOS complex by the ERK and JNK signaling pathways. *J. Biol. Chem.* **271,** 6328–6332 (1996).
29. Tanaka, H., Katoh, H. & Negishi, M. Pragmin, a novel effector of Rnd2 GTPase, stimulates RhoA activity. *J. Biol. Chem.* **281,** 10355–10364 (2006).
30. Ceulemans, H. & Bollen, M. Functional diversity of protein phosphatase-1, a cellular economizer and reset button. *Physiol. Rev.* **84,** 1–39 (2004).
31. Schmandt, R., Liu, S. K. & McGlade, C. J. Cloning and characterization of mPAL, a novel Shc SH2 domain-binding protein expressed in proliferating cells. *Oncogene* **18,** 1867–1879 (1999).
32. Pawson, T. & Nash, P. Assembly of cell regulatory systems through protein interaction domains. *Science* **300,** 445–452 (2003).
33. Charest, A., Wagner, J., Jacob, S., McGlade, C. J. & Tremblay, M. L. Phosphotyrosine-independent binding of SHC to the NPLH sequence of murine protein-tyrosine phosphatase-PEST. Evidence for extended phosphotyrosine binding/phosphotyrosine interaction domain recognition specificity. *J. Biol. Chem.* **271,** 8424–8429 (1996).
34. Sun, T. *et al.* Activation of multiple proto-oncogenic tyrosine kinases in breast cancer via loss of the PTPN12 phosphatase. *Cell* **144,** 703–718 (2011).
35. Croucher, D. R. *et al.* Involvement of Lyn and the atypical kinase SgK269/PEAK1 in a basal breast cancer signaling pathway. *Cancer Res.* **73,** 1969–1980 (2013).

Supplementary Information is available in the online version of the paper.

Acknowledgements We thank J. Moffat for shRNA lentiviruses and K. Shokat for PI3Kp110 isoform-specific inhibitors. We thank C. Jorgensen, R. Williams, I. Louria-Hayon, R. Tian, and E. Petsalaki for critical input, A. James, V. Nguyen, and B. Larsen for technical assistance and M. M. Stacey, C. Chen and J. Jin for comments on the manuscript. Supported by Genome Canada through the Ontario Genomics Institute, the Ontario Research Fund from the Ontario Ministry of Research and Innovation, a Terry Fox Foundation team grant, the Canadian Institutes of Health Research (MOP-13466-6849), and the Canada Foundation for Innovation. M.A.S. is supported by a Vanier Canada Graduate Studentship and R.B. is supported by a CIHR postdoctoral fellowship. Support for R.J.D. was from the National Health and Medical Research Council of Australia and Cancer Council New South Wales (NSW), and for D.R.C. from Cancer Institute NSW.

Author Contributions Y.Z. conceived and implemented the sMRM approach. C.Z., Y.Z. and L.T. developed and performed sMRM assays. S.A.T. provided technical MS support. Y.Z., M.A.S., N.S.D., D.R.C., R.B. and A.Y.D. performed biochemical and functional experiments. W.R.H. generated *Shc1*-deficient MEFs and *Grb2*$^{flox/flox}$ MEFs. Y.Z. and A.P. performed the computational analysis. T.P., R.J.D. and A.-C.G. oversaw the project. Y.Z., M.A.S., K.C. and T.P. wrote the paper with input from J.W.D.

Author Information Reprints and permissions information is available at www.nature.com/reprints. The authors declare competing financial interests: details are available in the online version of the paper. Readers are welcome to comment on the online version of the paper. Correspondence and requests for materials should be addressed to T.P. (pawson@lunenfeld.ca).

METHODS

Antibodies and reagents. We used anti-Flag M2 agarose (Sigma) for dt-Shc1 immunoprecipitation and anti-Shc1 (BD Biosciences) for immunoprecipitation of endogenous Shc1. We also used the following antibodies: anti-EGFR pY1073, anti-EGFR pY1068, anti-EGFR (Lifespan LS-C6640), anti-pAKT S473, anti-AKT, anti-MAPK p44/42, anti-Grb2 (CST). The MEK inhibitor PD 98059 and the PI(3)K inhibitor LY294001 were purchased from Cell Signaling Technology. The isoform specific PI(3)K inhibitors (PIK-90 and TGX221) were gifts from K. Shokat (UCSF). We also used the following recombinant proteins: AKT1 (GST-tagged, Cell Sciences, CRA004B), Src (Cell Sciences, CRS155A), MAPK1 (Millipore, 14-439), EGFR (Abnova, H00001956-P02), and PI(3)K (p110a/85a) (SignalChem, P27-18H-10). The phosphatase inhibitor cocktail set II (524625) and IV (524628) were purchased from Calbiochem.

Plasmid constructs and site-directed mutagenesis. The cDNA expressing p52Shc1 with N-terminal Flag and eGFP tags was cloned into the pCAGGS expression vector (at HindIII and EcoRI restriction sites). To generate Shc1 phosphorylation site mutants, we used the QuikChange Site-Directed Mutagenesis Kit (Stratagene) and the following primers (forward):

S29A: 5′-GGACCAGACACGGGGCCTTTGTCAATAAGCC-3′; T214A: 5′-ACCGAAGCTGGTCGCCCCCCATGACAG-3′; S335A: 5′-GCTGGGCCCCCAAATCCTGCTCTTAATGGCAGTGCACCC-3′; 3F (Y313F/Y239F/Y240F): first primer for Y239F/Y240F: 5′-CCCCCTGACCATCAGTTCTTCAATGACTTTCCAGGG-3′, and second primer for Y313F: 5′-TCTTCGATGACCCCTCCTTTGTCAACATCCAGAAT-3′.

Generating stable eGFP and Flag-tagged p52Shc1 (dt-Shc1)-expressing Rat-2 and MEF cell lines. Wild type Rat-2 fibroblasts and *Shc1*$^{-/-}$ MEFs were transfected with plasmid constructs expressing dt-Shc1 or its mutants using polyethylenimine. Cells were sorted in three rounds using FACS cycles, and divided into three pools based on the signal intensity of the eGFP fluorescence. The dt-Shc1 expression levels of the three pools of cells were examined by immunoblotting and compared with the level of endogenous p52Shc. A pool of cells expressing dt-Shc1 levels comparable to that of endogenous p52Shc1 were selected (Supplementary Fig. 1).

***In vitro* kinase assay.** MEFs were serum-starved for 2 h. dt-Shc1 was affinity purified using anti-Flag M2-conjugated agarose followed by washing 4 times with lysis buffer. The beads were equally divided into four aliquots and washed twice with relevant kinase buffers (buffer A (for Erk and AKT): 25 mM Tris-HCl, pH 7.5, 5 mM beta-glycerophosphate, 0.5 mM DTT (dithiothreitol), 0.1 mM Na_3VO_4, 10 mM $MgCl_2$, 1 mM EGTA, 50 nM calyculin A, 20 μM ATP; buffer B (for Src), 5 mM $MnCl_2$ was added into buffer A). Purified recombinant human Src (100 ng), Erk (100 ng), AKT1 (100 ng), or kinase buffer was added to the beads and incubated for 30 min at 37 °C. The reactions were stopped by washing the beads once with 50 mM EDTA and twice with 50 mM ammonium bicarbonate. The beads were then digested with 0.4 μg trypsin overnight at 37 °C and the phosphorylation sites on Shc1 were quantified by sMRM.

Proliferation assay. *Shc1*$^{-/-}$ MEFs reconstituted with dt-Shc1 or its mutants were seeded in quadruplicate at 0.5×10^4 cells per well into 24-well plates. Cells were trypsinized and the cell number was counted using a hemocytometer every 24 h over a 7-day period.

Inducible deletion of Grb2 in MEFs. The *Grb2* conditional allele was generated by flanking exon 2 of *Grb2* with floxP sites to introduce a frameshift (Supplementary Fig. 18). MEFs were expanded from E13.5 *Grb2*$^{flox/flox}$ embryos and immortalized by the 3T3 protocol as previously described[36]. The immortalized *Grb2*$^{flox/flox}$ 3T3 MEF line was then infected with pMSCV-CreER retrovirus, and selected with 5 μg ml^{-1} blasticidin in DMEM supplemented with 10% FBS to generate a stable pool of CreER-expressing *Grb2*$^{flox/flox}$ 3T3 MEFs. For inducible deletion of *Grb2*, 4-OH tamoxifen (1 μg ml^{-1}) was added into the culture medium for 48 h. The deletion of *Grb2* expression was confirmed by immunoblotting.

Lentivirus-mediated gene knockdown. Lentiviral shRNAs specifically targeting human *SGK269* and *DAB2IP* genes were provided by J. Moffat. shRNA sequences used were as follows:

SGK269 (accession: NP_079052): shRNA1: 5′-CCACAAGTGTAATAAGCCATA-3′; shRNA2: 5′-GAAGATCTCTTCCAGACTTTC-3′;

DAB2IP (accession: Q5VWQ8): 5′-GACTCCAAACAGAAGATCATT-3′

Lentiviruses were produced as previously described[37] and used to infect HeLa cells for 24 h, followed by puromycin (2μg ml^{-1})-mediated drug selection for 5 days. Knockdown efficiency was judged by quantifying the relative amount of targeted protein in the Shc1 complex after EGF stimulation in pooled colonies using sMRM.

Matrigel assay. MCF10A cells overexpressing SgK269(WT), SgK269(Y1188F) or the control plasmid were grown in Matrigel for 12 days, as previously described[38]. The resulting acini were photographed and the diameters of ~100 acini were measured using ImageJ (± s.e.m., $^{**}P < 0.0001$, $^{*}P < 0.001$). Acinar morphology was determined by visual inspection (± s.d., $n = 2$).

Shc1 immunoprecipitation and on-bead tryptic digestion. Cell lines expressing dt-Shc1 were seeded at 1×10^7 cells per 15 cm dish (Nunc) in DMEM plus 10% FBS. The following day, the indicated treatments were applied to the cells and they were immediately washed three times with ice-cold PBS to quench cell signaling, then lysed in NP40 lysis buffer (50 mM HEPES-NaOH, pH 8, 150 mM NaCl, 1 mM EGTA, 0.5% NP40, 100 mM NaF, 2.5 mM $MgCl_2$, 10 mM $Na_4P_2O_7$, 1 mM DTT, 10% glycerol) supplemented with protease and phosphatase inhibitors (50 mM β-glycerolphosphate, 10 μg ml^{-1} aprotinin, 10 μg ml^{-1} leupeptin, 1 mM Na_3VO_4, 100 nM calyculin A, 1 mM PMSF (phenylmethylsulphonyl fluoride)). The total cell lysates were centrifuged at 20,800*g* for 30 min to pellet the nuclei and insoluble material. Nuclear-free lysates were pre-cleared by one-hour incubation with protein A sepharose and normalized for total protein concentration using the Bio-Rad protein assay. dt-Shc1 was immunoprecipitated by incubating lysates with 5 μl (bed volume) anti-Flag M2 antibody-conjugated agarose for 4 h at 4 °C. The beads were washed 4 times with lysis buffer and twice with 50 mM ammonium bicarbonate (ABC) before resuspending in 20 μl ABC (50 mM). Tryptic digestion was performed by directly adding trypsin (enzyme : substrate ~ 1 : 50) to the beads and incubating at 37 °C overnight. The digestion was stopped by adding 3% formic acid to the reaction and the supernatant was transferred into a clean tube and dried.

Mass spectrometry analysis of the Shc1 interactome. Dried tryptic samples were reconstituted with 3% formic acid in HPLC grade water. Samples were loaded on to a 75 μm inner diameter (ID)/360 μm outer diameter (OD) pulled tip packed with 3 μm ReproSil C18 and analysed on an TripleTOF 5600 mass spectrometer (AB SCIEX) or a QSTAR Elite mass spectrometer (AB SCIEX), each coupled to an Eksigent nanoLC Ultra 1D plus pump with a flow rate of 200 nl per min and a gradient of 2% to 35% acetonitrile over 90 min. The mass spectrometers were operated in information-dependent acquisition mode. For the TripleTOF 5600, a cycle time of 1.3 s was employed using a survey TOF scan of 250 ms (msec) at ~ 30,000 resolution followed by selection of the top 20 most intense peptides for MS/MS for 50 ms each with high sensitivity (at ~ 18,000 resolution). Only peptides with a charge state above +1 were selected for MS/MS and dynamic exclusion was set to 15 s for all ions within 20 p.p.m. For the QSTAR Elite, a cycle time of 5.25 s was employed using a survey TOF scan of 250 ms at ~ 10,000 resolution followed by selection of the top 5 most intense peptides for MS/MS using a fragment intensity multiplier of 8 and a maximum accumulation time of 1 s for each candidate. Enhance All was used for all MS/MS scans. Only peptides with a charge state above +1 were selected for MS/MS and dynamic exclusion was set to 20 s for all ions within 50 p.p.m. Q1 was set to Unit resolution on all MS/MS scans for both the TripleTOF 5600 and the QSTAR Elite.

All acquired raw files were converted to mgf format and searched against Ensembl databases (rat and mouse—release 44) using Mascot version 2.1 or ProteinPilot version 2.0.1 (AB SCIEX). The following parameters were used for the database searches, precursor mass accuracy: 30 p.p.m.; MS/MS mass accuracy 0.1 Da for Elite and 0.05 Da for Triple TOF 5600, and modifications were the following: phospho-S/T/Y (variable), methionine oxidation (variable), and NQ deamidation (variable); one missed trypsin cleavage was accepted. All peptides with a Mascot score over 25 were selected for sMRM method building.

sMRM assay construction and optimization. The sMRM assay uses specific peptides and their fragments (termed transitions) as unique discriminators of individual proteins. Based on the fragmentation information acquired from the initial MS/MS scans, we built the sMRM assay to specifically quantify the Shc1 interactome. The MS/MS information from previous information-dependent acquisition (IDA) experiments were imported by the MRMpilot 1.1 (AB SCIEX) software to generate a list of potential sMRM transitions which was then manually filtered to contain only fragments ions greater than the precursor that were generated from doubly or triply charged precursor peptides with no methionine or tryptophan residues, and no N-terminal glutamine residues in general. However, for certain peptides, such as phosphopeptides, containing chemically unstable but biologically significant residues that could not be excluded from the list, the dominant forms of the peptide transition species were measured.

For confident peptide identification and quantification, at least three peptides per protein and a minimum of two transitions per peptide were targeted for sMRM analysis. The initial sMRM transition list then underwent multiple rounds of validation and optimization using non-scheduled MRM analysis of Shc1 immunoprecipitates. Transitions that showed low sMRM detection sensitivity were removed. Proteins that failed to produce a minimum of two unique peptides with sufficient detection sensitivity were not examined further. The peptide retention times were determined by MS/MS from multiple MRM initiated detection and sequencing (MIDAS) runs using MultiQuant (version 2.1) software[39]. The final

sMRM method consists of 381 transitions from 171 unique peptides, corresponding to 30 proteins (including Shc1) from the Shc1 interactome.

For data normalization, we chose 5 Shc1 peptides that were unlikely to either undergo post-translational modifications, other than oxidation on Met, Trp and His residues, or produce analytical artefacts (such as isobaric interference) (Supplementary Fig. 3a). These peptides showed linear responses over the concentration range of the samples (Supplementary Fig. 3b). Each biological experiment was measured with two technical repeats and a logistic regression analysis (LRA) showed low variation between the two measurements (Supplementary Fig. 4a, b). We also spiked 100 fmol of digested α-casein into all samples as an analytical standard to monitor the LC–MS performance (Supplementary Table 4).

sMRM quantification. sMRM analysis was performed on hybrid triple quadrupole/ion trap mass spectrometers (4000QTrap and 5500QTrap; AB SCIEX). Chromatographic separations of peptides were carried out on a nano-LC system (Eksigent) coupled to a 100 μm ID fused silica column packed with 5 μm ReproSil C18 as a trap column and a 75 μm ID. fused silica column packed with 3 μm ReproSil C18 as the separation column. A micro Tee was used to connect both columns and a micro-union was used to connect the columns to an emitter. Peptides were separated with a linear gradient from 2–30% acetonitrile in 90 min at a flow rate of 300 nl min^{-1}. The MIDAS workflow was used for sMRM transition confirmation. For all runs, the MS instrument was operated in the positive mode. LC–MS conditions, for all experiments, were evaluated using a 30 min gradient run of a mixture of 30 fmol of BSA and 60 fmol of α-casein (72 MRM transitions) before each sample run. In order to reduce the carry over, at least one clean-up run and one BSA run were performed between samples. Each sMRM run was scheduled using previously determined LC retention times with a 5-min MRM detection window and a 3-s scan time with both Q1 and Q3 settings at unit resolution. We injected each biological sample at least twice for increased quantification confidence. In general, the technical replicates showed little variations (Supplementary Fig. 4).

sMRM data processing. The MS/MS spectra acquired by MIDAS were first searched against relevant Ensembl databases using Mascot to confirm the identities of peptides. The raw data was then imported into MultiQuant v2.1 (AB SCIEX) for automatic MRM transition detection followed by manual inspection by the investigators to increase confidence. Subsequently, the eXtracted ion chromatogram (XIC, the peak area) of each transition was calculated. The XIC of each transition is proportional to the real quantity (abundance) of the corresponding peptide. The data were visualized and exported as Excel spreadsheets using MarkerView 1.2.1 (AB SCIEX) into a custom developed SQL based data-storage and management system (CoreFlow) for further analysis. sMRM quantification data sets from this study can be found at (http://pawsonlab.mshri.on.ca/Shc1_dynamics).

Statistical analysis. We used the R statistical package[40,41] for generating the pseudo-3D view (dot blots) of the temporal and spatial profiles of Shc1 interactome and for the PCA analysis.

To calculate the relative abundance (RA) of each protein or phosphopeptide in Shc1 immunoprecipitates, the mean XIC of a given sMRM transition from technical replicates was normalized to the Shc1 protein level. The normalized value was then converted to a percentage, using the highest value of that transition in a given experiment as 100. Percentages from all of the transitions representing the same protein or phosphopeptide were averaged and presented as RA ± s.d. RA values for Shc1-interacting proteins from wild-type cells as compared to cells expressing mutated *Shc1* or *Grb2* genes were calculated slightly differently. Here, the highest XIC value of a given transition measured in the wild-type cells was set to 100. Dot blots were generated from the RA values using a mixture of the R Lattice package functions xyplot, bwplot and levelplot.

Principal component analysis (PCA) was applied to the RA values using the 'princomp' function in R with parameters "corr = TRUE" and "scale=T". We selected the first 2 or 3 main components from the PCA, which accounted for more than 80% of the variation of the data intercorrelation.

36. Rittling, S. R. Clonal nature of spontaneously immortalized 3T3 cells. *Exp. Cell Res.* **229,** 7–13 (1996).
37. Moffat, J. *et al.* A lentiviral RNAi library for human and mouse genes applied to an arrayed viral high-content screen. *Cell* **124,** 1283–1298 (2006).
38. Brummer, T. *et al.* Increased proliferation and altered growth factor dependence of human mammary epithelial cells overexpressing the Gab2 docking protein. *J. Biol. Chem.* **281,** 626–637 (2006).
39. Unwin, R. D., Griffiths, J. R. & Whetton, A. D. A sensitive mass spectrometric method for hypothesis-driven detection of peptide post-translational modifications: multiple reaction monitoring-initiated detection and sequencing (MIDAS). *Nature Protocols* **4,** 870–877 (2009).
40. R Development Core Team. A Language and Environment for Statistical Computing. R Foundation for Statistical Computing. http://www.R-project.org (2010).
41. Sarkar, D. *Lattice: Multivariate Data Visualization with R* (Springer, 2008).